Study of the dynamics of poly(ethylene oxide) by combining molecular dynamic simulations and neutron scattering experiments

M. Brodeck, F. Alvarez, A. Arbe, F. Juranyi, T. Unruh, O. Holderer, J. Colmenero, and D. Richter

Citation: The Journal of Chemical Physics **130**, 094908 (2009); doi: 10.1063/1.3077858

View online: https://doi.org/10.1063/1.3077858

View Table of Contents: http://aip.scitation.org/toc/jcp/130/9

Published by the American Institute of Physics

Articles you may be interested in

Polymer dynamics under cylindrical confinement featuring a locally repulsive surface: A quasielastic neutron scattering study
The Journal of Chemical Physics **146**, 203306 (2017); 10.1063/1.4974836

A Theory of the Linear Viscoelastic Properties of Dilute Solutions of Coiling Polymers
The Journal of Chemical Physics **21**, 1272 (1953); 10.1063/1.1699180

Dynamics of entangled linear polymer melts: A molecular-dynamics simulation
The Journal of Chemical Physics **92**, 5057 (1990); 10.1063/1.458541

Neutron scattering study of the dynamics of a polymer melt under nanoscopic confinement
The Journal of Chemical Physics **131**, 174901 (2009); 10.1063/1.3258329

A comparison of united atom, explicit atom, and coarse-grained simulation models for poly(ethylene oxide)
The Journal of Chemical Physics **124**, 234901 (2006); 10.1063/1.2204035

Time and length scales of polymer melts studied by coarse-grained molecular dynamics simulations
The Journal of Chemical Physics **117**, 925 (2002); 10.1063/1.1481859

PHYSICS TODAY
WHITEPAPERS

ADVANCED LIGHT CURE ADHESIVES

Take a closer look at what these
environmentally friendly adhesive
systems can do

READ NOW

PRESENTED BY
MASTERBOND
ADHESIVES | SEALANTS | COATINGS

THE JOURNAL OF CHEMICAL PHYSICS **130**, 094908 (2009)

Study of the dynamics of poly(ethylene oxide) by combining molecular dynamic simulations and neutron scattering experiments

M. Brodeck,[1] F. Alvarez,[2,3] A. Arbe,[2,a)] F. Juranyi,[4] T. Unruh,[5] O. Holderer,[1]
J. Colmenero,[2,3,6] and D. Richter[1]
[1]*Institut für Festkörperforschung, Forschungszentrum Jülich GmbH, D-52425 Jülich, Germany*
[2]*Centro de Física de Materiales (CSIC-UPV/EHU), Apartado 1072, 20080 San Sebastián, Spain*
[3]*Departamento de Física de Materiales UPV/EHU, Apartado 1072, 20080 San Sebastián, Spain*
[4]*Laboratory for Neutron Scattering, ETH Zurich and PSI, CH-5232 Villigen PSI, Switzerland*
[5]*Forschungsneutronenquelle Heinz Maier-Leibnitz (FRM II), 85747 Garching, Germany*
[6]*Donostia International Physics Center, Paseo Manuel de Lardizabal 4, 20018 San Sebastián, Spain*

(Received 19 November 2008; accepted 6 January 2009; published online 6 March 2009)

We performed quasielastic neutron scattering experiments and atomistic molecular dynamics simulations on a poly(ethylene oxide) (PEO) homopolymer system above the melting point. The excellent agreement found between both sets of data, together with a successful comparison with literature diffraction results, validates the condensed-phase optimized molecular potentials for atomistic simulation studies (COMPASS) force field used to produce our dynamic runs and gives support to their further analysis. This provided direct information on magnitudes which are not accessible from experiments such as the radial probability distribution functions of specific atoms at different times and their moments. The results of our simulations on the H-motions and different experiments indicate that in the high-temperature range investigated the dynamics is Rouse-like for Q-values below ≈ 0.6 Å^{-1}. We then addressed the single chain dynamic structure factor with the simulations. A mode analysis, not possible directly experimentally, reveals the limits of applicability of the Rouse model to PEO. We discuss the possible origins for the observed deviations. © *2009 American Institute of Physics*. [DOI: 10.1063/1.3077858]

I. INTRODUCTION

Poly(ethylene oxide) (PEO) is found ubiquitously in a variety of applications. One of the most exploited ones is its use as polymer electrolyte,[1,2] but it can also be employed for many other very different purposes, such as in the cosmetic and pharmaceutical fields.[3–5]

Recently, this homopolymer has also drawn attention for its dynamic behavior in miscible blends with polymers of much higher glass transition temperatures T_g, such as poly(methyl methacrylate)[6–22] and poly(vinyl acetate).[21,23,24] This is due to the rather unusual dynamics displayed by PEO in such blends, which could be attributed to confinement effects induced by the rigid high-T_g-component. In fact, PEO has also been a focus of interest for studying confinement effects under different conditions, such as e.g., in nanocomposites.[25,26] Obviously, the proper characterization of the deviations from the bulk behavior of PEO under different confinement situations demands the detailed knowledge of the structural and dynamical properties of the neat polymer at a molecular scale. This can be provided by the combination of neutron scattering experiments and molecular dynamics (MD) simulations. The complementary use of these techniques has proven to be an extremely successful route to address a number of similar problems in the field of soft matter.[7,27–39]

Regarding MD simulations on PEO, a relatively large number of publications can be found in literature.[25,26,40–57,60] Some of them deal mainly with structural properties,[48,50,51,53–56,60] but the local dynamics is also addressed in others;[42,52,57] sometimes the works have been motivated by its use as polyelectrolyte[40,41,49] or have been focused on its confined behavior.[25,26,42] Always fully atomistic models have been investigated, except in the case of Refs. 49 and 55 where united atom simulations were performed. In a recent work,[43] PEO has also been used as model system to apply different levels of coarse graining. However, to our knowledge, the information contained in the simulations has never been used to realize a detailed Rouse mode analysis. In this work, after the thorough validation of the MD simulations by direct comparison with neutron diffraction data and results on the coherent and incoherent structure factors, we address the question of the single chain dynamics of this flexible polymer and investigate the limits of applicability of the widely accepted Rouse model. In this way, we also contribute to a general problem of polymer physics.

In Sec. II we will describe the experimental techniques used here and present the corresponding results. Thereafter we give the details on our fully atomistic MD simulations. In particular, we comment on problems with the condensed-phase optimized molecular potentials for atomistic simulation studies (COMPASS) force field where modifications are needed for the standard default value of a splinewidth parameter concerning the cutoff evaluation behavior of Coulombic interactions. In Sec. IV the direct comparison of simulation and experimental results validate the simulated cell. In the

---

[a)] Author to whom correspondence should be addressed. Electronic mail: a.arbe@ehu.es.

discussion we first address magnitudes that cannot be experimentally accessed, such as mean squared displacements (MSDs) of specific atoms. The experimental and simulation results evidence the observation of Rouse-like dynamics in PEO up to rather high Q-values in the investigated temperature range. We analyze in detail the Rouse-mode correlators computed on the simulated chains and discuss the limits of the Rouse model for this system. In particular, by evaluating Rouse relaxation rates and Rouse-mode amplitudes, we show that the monomeric friction coefficient displays a strong mode dependency.

II. EXPERIMENTS

A. Samples

The samples investigated in this work were fully protonated (hPEO) and fully (99.8%) deuterated (dPEO) polymers. The molecular weights were $M_n^{\mathrm{hPEO}}=24\ \mathrm{kg/mol}$ and $M_n^{\mathrm{dPEO}}=36\ \mathrm{kg/mol}$. The polydispersities M_n/M_w were of 1.03 for hPEO and 1.04 for dPEO. The samples show T_g-values of ≈ 220 K. The melting point of PEO is about 338 K. Further details on the synthesis of these polymers can be found in Ref. 58.

B. Neutron scattering

The number of neutrons that are scattered from a sample after having exchanged an energy $\Delta E=\hbar\omega$ and momentum $\vec{Q}=\vec{k}_f-\vec{k}_i$ originate either from incoherent or from coherent scattering. In the cross sections the incoherent scattering function $S_{\mathrm{inc}}^{\alpha}(Q,\omega)$, corresponding to the type of nucleus $\alpha(\mathrm{H,C,O,D},\ldots)$, is weighted by the corresponding incoherent cross section $\sigma_{\mathrm{inc}}^{\alpha}$. For isotropic samples $S_{\mathrm{inc}}^{\alpha}(Q,\omega)$ is connected to the self-part of the van Hove correlation function, $G_{\mathrm{self}}^{\alpha}(r,t)$,

$$G_{\mathrm{self}}^{\alpha}(r,t)=\frac{1}{N_\alpha}\left\langle \sum_{i\alpha}^{N_\alpha}\delta(r-|\vec{r}_{i\alpha}(t)-\vec{r}_{i\alpha}(0)|)\right\rangle, \tag{1}$$

by a double Fourier transformation in space and time. N_α is the number of nuclei of type α and i is the index of the atom. This function is, in the classical limit, the probability for an atom of the α-kind to move by a distance r in a given time t. In contrast, coherent scattering arises from relative positions of atomic pairs at different times and, therefore, reflects the collective dynamics of a system. The coherent double differential cross section is given by

$$\left(\frac{\partial^2\sigma}{\partial\Omega\,\partial E}\right)_{\mathrm{coh}}\propto\left\langle\sum_{\alpha,\beta}\sum_{i\alpha,j\beta}^{N_\alpha,N_\beta}b_{\mathrm{coh}}^{\alpha}b_{\mathrm{coh}}^{\beta}\frac{1}{2\pi\hbar}\int_0^\infty dt\; e^{-i\omega t}e^{i\vec{Q}[\vec{r}_{i\alpha}(t)-\vec{r}_{j\beta}(0)]}\right\rangle,$$

where $b_{\mathrm{coh}}^{\alpha}$ is the scattering length of the α-isotope. Integrated over all possible energy transfers, the double differential cross section is composed of the static structure factor from coherent scattering together with a Q-independent incoherent contribution (equivalent to $t=0$).

The differences in the cross sections of the involved isotopes allow highlighting specific contributions in the scattered intensity by choosing different levels of deuteration. Since $\sigma_{\mathrm{inc}}^{\mathrm{H}}$ (80.27 b) is significantly higher than all other cross sections ($\sigma_{\mathrm{inc}}^{\mathrm{C,O}}=0$, $\sigma_{\mathrm{coh}}^{\mathrm{H,C,O}}<5.6$ b) in PEO, a protonated sample is ideal for a direct investigation of the self-motion of hydrogen atoms. On the other hand, the investigation of a deuterated sample focuses on the collective properties of a system. Moreover, as the values of $b_{\mathrm{coh}}^{\alpha}$ are very similar to the isotopes conforming a deuterated sample (C,D,O), the different partial correlation functions contributing to the coherently scattered intensity are almost equally weighted, thus delivering the true or total dynamic structure factor.

1. Time of flight

In the microscopic time region, the self motion of PEO protons were investigated by the time-of-flight (ToF) spectrometer FOCUS at the spallation source SINQ (Paul Scherrer Institut, Villigen) using a fully protonated sample (hPEO). The collective dynamics was studied using the fully deuterated dPEO at the high resolution ToF spectrometer TOFTOF at the neutron source FRM II (Neutronenquelle Heinz Meier-Leibnitz, Garching).

ToF measurements yield the energy-resolved scattering at different angles. After correcting the change in the Q-vector due to the change of the neutrons energy, the quasielastic spectrum at a given Q-value is obtained.

FOCUS: The 400 ^{3}He countertubes in three banks detect the scattered neutrons after passing a 2.5 m flight distance filled with argon. Thereby, the scattering angles covered the range between 10° and 130°. Using and incident wavelength $\lambda=5$ Å, the energy resolution of the experiment was δE (half width at half maximum HWHM) $\approx 45\ \mu$eV. The hPEO sample was placed into a hollow aluminum cylinder of 12 mm diameter, providing a transmission of about 90%. We investigated temperatures of 350, 375, and 400 K, with measuring times of the order of 8 h each. The resolution was determined from a measurement of the sample at 20 K. Background corrections were performed by subtracting the intensity scattered by the empty cell. The detector efficiency was corrected by the measurement of a vanadium sample of 1.2 mm thickness with the same geometry. After interpolating the signal at constant Q in a reasonable energy transfer region, the effective Q-range was reduced to values between 0.50 and 2.2 Å^{-1}.

Figure 1 shows the FOCUS results for four of the

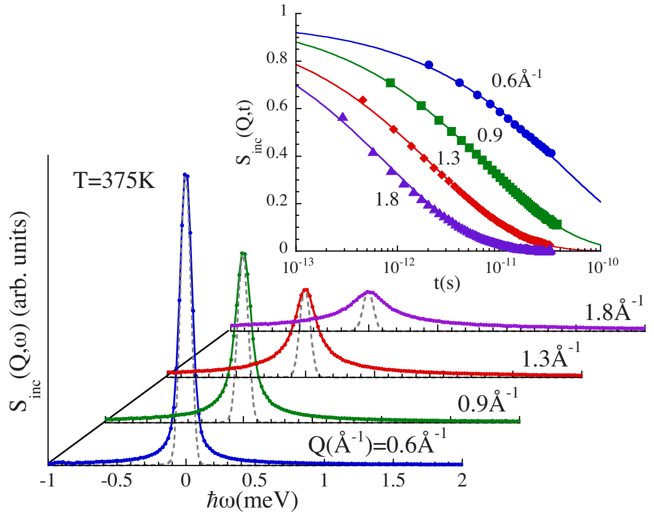

FIG. 1. (Color online) Spectra obtained with FOCUS (hPEO) at $T = 375$ K and the Q-values indicated. The Fourier transformed data are shown in the inset (lines: KWW fits).

Q-values investigated at 375 K. Due to the convolution with the instrumental resolution and the influence of the fast dynamical processes[59] (below ≈ 2 ps) on the scattering functions in frequency domain, it is difficult to determine their exact functional form. Therefore, it is convenient to Fourier transform them into the time domain. In this way, the resolution effect can easily be corrected by simple division of the Fourier transformed spectrum by that of the reference measurement corresponding to a purely elastic signal (in this case, the PEO sample at 20 K).

The intermediate scattering functions obtained from the spectra in Fig. 1 are shown in the inset of the figure. As can be seen, after ≈ 1 ps they can be well described by a stretched exponential or Kohlrausch–Williams–Watts function (KWW),

$$\phi_{\mathrm{KWW}}(t) = A \exp\left[-\left(\frac{t}{\tau_W(Q,T)}\right)^{\beta}\right], \tag{2}$$

with a fixed value of the shape parameter β equal to 0.5. The time scales $\tau_W(Q)$ resulting from these fits [denoted as $\tau_{\mathrm{self}}(Q)$ since they reflect H self-motions] are shown in Fig. 2 as filled symbols. For $Q \lesssim 1$ Å^{-1} the characteristic time decays with the scattering vector as $\tau_{\mathrm{self}} \propto Q^{-4}$.

TOFTOF: This spectrometer covers scattering angles ranging from $-15°$ to $140°$. For our measurements of dPEO, we set the wavelength of the incident beam to $\lambda = 5.1$ Å and achieved an energy resolution of $\delta E(\mathrm{HWHM}) \approx 50$ μeV by adjusting the frequency of the choppers. The sample was placed in a flat 4 mm Nb container with 3 mm of aluminum plates to obtain a thickness of 1 mm. The edge of the container was oriented to face to 45°. This geometrical setup forced us to disregard data collected by the detectors with an angle smaller than 60°, which led to an effective Q-range of 1.4–2.2 Å^{-1}. Each of the temperatures (350, 375, and 400 K) was measured for 5 h. The resolution was determined using vanadium and an empty cell was measured for background corrections. Some of the spectra collected at $T = 375$ K are shown in Fig. 3.

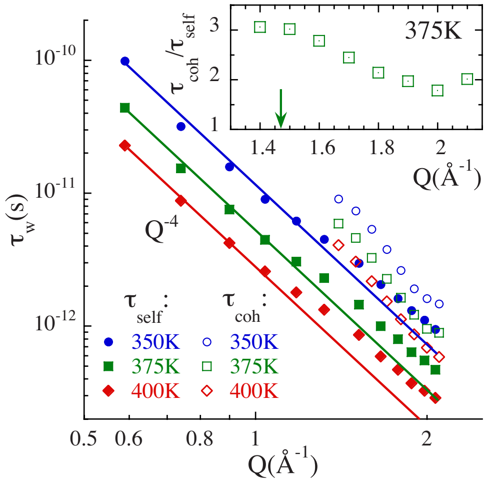

FIG. 2. (Color online) Momentum transfer dependence of the characteristic times obtained from the KWW fit of the Fourier transformed incoherent (τ_{self}, full symbols) and coherent (τ_{coh}, empty symbols) scattering functions at the temperatures investigated. Solid lines indicate a Q^{-4}-dependence. Inset: ratio between the coherent and incoherent time scales for 375 K. The arrow shows the position of the maximum of the static structure factor.

Following an analogous procedure as for incoherent scattering, we Fourier transformed the TOFTOF data. A stretched exponential function [Eq. (2)] has then been fitted to these data with β fixed to be 0.5 (see inset of Fig. 3). Figure 2 shows the resulting times of these fits $\tau_{\mathrm{coh}}(Q)$ together with those deduced for the H self-motions. The collective times are significantly slower than the incoherent ones. This can be well appreciated in the inset of Fig. 2, where the ratio between both time scales has been represented for 375 K. This ratio is maximum in the low-Q range explored. We note that the structure factor of PEO shows its first peak at around 1.5 Å^{-1} (see later Ref. 60). For simple monoatomic liquids the so-called deGennes narrowing[61] predicts a Q-dependence for collective motions, $\tau_{\mathrm{coh}} = \tau_{\mathrm{self}} S(Q)$. Thus, for PEO the coherent time scales should also be somehow modulated by the structure factor of the system, thereby reflecting some degree of collectivity.

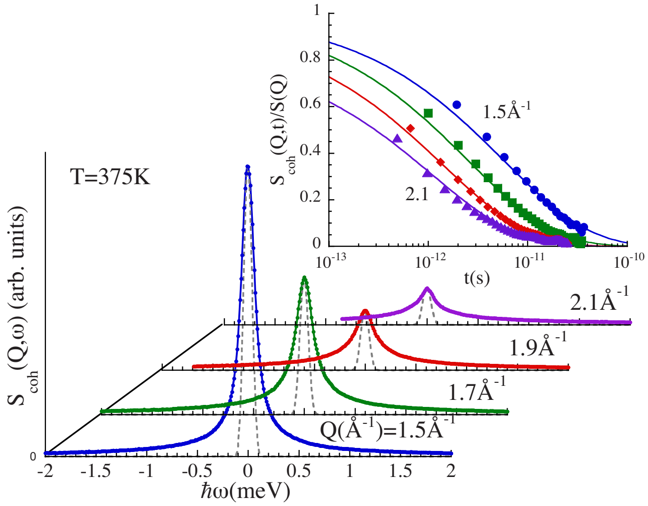

FIG. 3. (Color online) Spectra obtained with TOFTOF (dPEO) at $T = 375$ K and the Q-values indicated. The Fourier transformed data are shown in the inset (lines: KWW fits).

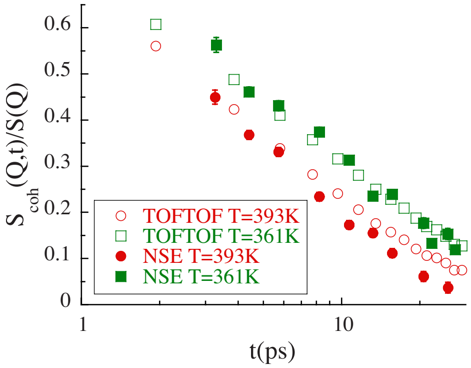

FIG. 4. (Color online) Direct comparison of Fourier transformed TOFTOF data (empty symbols) with NSE results at $Q=1.5$ Å^{-1} and two temperatures. The TOFTOF points have been interpolated to the NSE temperatures using the three measured temperatures of 350, 375, and 400 K.

2. Neutron spin echo

This technique is unique in that it offers the scattering functions directly in the time domain.[62] Since the incoherent scattering process flips the spin of 2/3 of all neutrons, only 1/3 contribute to the echo signal, while the rest is background. Because of the spin flip, the echo is inverted and its amplitude has to be subtracted from the one obtained from coherent scattering. The measured variable is therefore given by

$$\frac{S(Q,t)}{S(Q,0)}=\frac{S_{\text{coh}}(Q,t)-\frac{1}{3}S_{\text{inc}}(Q,t)}{S_{\text{coh}}(Q,0)-\frac{1}{3}S_{\text{inc}}(Q,0)}. \tag{3}$$

The neutron spin echo (NSE) method was used to measure collective dynamics on deuterated PEO (J-NSE at the FRM II). Using a wavelength of $\lambda=5.0$ Å, three Q-values at and around the structure factor peak were investigated at 361 and 393 K (1.3, 1.5, and 1.7 Å^{-1}). Using the instrument in *short-time mode* (turning off the currents in the main coils), we were able to access Fourier times down to about 3 ps. The dPEO sample (1 mm thickness) was placed in a Nb container. Measurements of a titanium-zirconium alloy were used as reference.

It can be shown that the contributions by incoherent scattering to the resulting NSE signal [see Eq. (3)] are negligible; also insignificant are those contributing to the TOFTOF spectra (this time in an additive way). Therefore, we can directly compare the normalized scattering function measured by NSE with the Fourier transformed spectra we obtained from the TOFTOF experiments (Fig. 4). As can be seen in this figure, the agreement is excellent. This comparison strongly supports the reliability of the Fourier transformation procedure used for the ToF data.

3. Backscattering

In this work we will refer to previously reported backscattering experiments on protonated PEO.[7,23] Those measurements were performed at the spectrometers BSS (Forschungsreaktor Jülich)[7] and IN16 (Institut Laue-Langevin, Grenoble).[23] With Si(111) monochromators these instruments provide an energy resolution of δE(HWHM) ≈ 0.45 μeV. Flat samples leading to transmissions of about 90% were investigated in both cases. The BSS results could be analyzed in the Q-range between 0.16 and 0.56 Å^{-1} for 350, 375, and 400 K. At 350 K, the Q-range was extended up to 0.97 Å^{-1} by IN16. At higher Q-values the spectra were out of the dynamic windows (better resolved with the wider energy window of ToF spectrometers). Further experimental details can be found in Refs. 7 and 23.

III. MD SIMULATIONS

The simulations were carried out using MATERIALS STUDIO 4.1 and the DISCOVER-3 module (version 2005.1) from Accelrys with the COMPASS force field. Most parameters of this field were derived based on *ab initio* data and later optimized empirically to yield good agreement with experiments. The functional form includes terms that can be divided into two categories: valence terms including diagonal and off-diagonal cross-coupling terms and nonbonded interaction terms. The valence terms represent internal coordinates of bond, bond-angle, torsion angle, and out of plane angle. The cross-coupling terms include combinations of two or three internal coordinates and are important for predicting vibration frequencies and structural variations associated with conformational changes. The analytical expression employs quartic polynomials for bond stretching and angle bending and a three-term Fourier expansion for torsions. The nonbonded interaction terms include a Coulombic function for the electrostatic interaction and a Lennard-Jones 6–9 function, rather than the more customary Lennard-Jones 6–12, for the van der Waals term. More information about this kind of force field, including the complete analytical expression for the functional form, can be found in Refs. 63 and 64. In order to compute the infinite range of the electrostatic interaction, the Coulombic terms have to be approximated by a group-based spherical cutoff method. For a given atom only those correlations within a certain radius are regarded; this value is known as the cutoff radius and in our case was set to be 12 Å. To avoid an unphysical jump at the border of the cutoff radius the energy is usually multiplied with a switching function to slowly decrease the potential to zero yielding a continuous potential energy and force. The standard size of this region is 1.0 Å, a value that produces correct results for most polymers. However, because of the oxygen atoms in PEO with their high partial charges, strong artificial forces emerge within this spline region since the potential still has a significant value at these distances. This problem can be solved by either completely removing the spline region and creating an energy jump at the cutoff radius or increasing the width of this region. We tested several options and compared the dynamic behavior of the system with results obtained using the Ewald summation method.[65] It was found that choosing a spline region of the same size as the cutoff radius (that is starting to spline the potential from $r=0$ to 12 Å) yields the best agreement. Artificial forces are suppressed and no energy jumps appear in the potential. At the same time this means that the complete potential function for the Coulombic interaction is artificially changed by the spline function. Nevertheless, we have chosen to follow this approach and were affirmed by the good agreement between experiments and simulations.

The simulated system was built by means of the well known amorphous cell protocol, which was proposed for the first time by Theodorou and Suter.[66,67] A cubic cell containing five polymer chains of 43 monomer units of ethylene oxide was constructed at 400 K under periodic boundary conditions, with a density fixed to be 1.0440 $\mathrm{g/cm^3}$ (experimental value), which leads to a cell size of 24.706 Å. After the creation of the cell, standard minimization procedures (Polak–Ribière conjugated gradients method) were followed in order to minimize the so obtained energy structure, and a subsequent dynamics was run for 2 ns in order to equilibrate the sample. The chosen temperatures were high enough to allow local structural equilibration of the sample in this time.[68] The system obtained in this way was used as a starting point for collecting data every 0.01 ps during a MD run of 1 ns. As an integration method we used the velocity-Verlet algorithm with a time step of 1 fs. The simulations were carried out in the NVT ensemble (i.e., keeping constant the number of atoms, the volume and the temperature). However, instead of a standard temperature-bath coupling (Nosé–Hoover or Berendsen thermostats, for instance) in order to control the temperature, we followed a rather crude velocity scaling procedure but with a wide temperature window of 10 K. Under these conditions, greater temperature fluctuations are allowed but the trajectory is usually less disturbed. In fact, for different polymer systems, we indeed checked that, by following this simple procedure, we obtained results similar to those obtained with a NVE ensemble (that is, keeping constant the sample total energy instead of its temperature), which has the proper Newtonian dynamics. After the first data collection of a 1 ns MD run, two more successive runs of 2 and 100 ns were carried out, collecting data every 0.05 and 0.5 ps, respectively. The same system was used to yield corresponding cells at different lower temperatures, namely, 350 and 375 K. In order to do this the cell was simply scaled to correspond to the new experimental density at the given temperature. NVT simulation runs of at least 2 ns were used to readapt the system to each new temperature before collecting data.

Although the COMPASS force field is able to parametrize deuterium atoms, we decided to simulate fully protonated samples in all cases. For the following comparison with deuterated experimental data, we simply used the different scattering lengths for the corresponding isotopes. The justification of this is based on the fact that such a procedure yielded good agreements in the past among simulations of different polymeric systems, obtained by means of the polymer consortium force field (PCFF), without an explicit dynamic parametrization for deuterium atoms. Moreover, we checked within the COMPASS force field and on the given system that the difference in structure data is nonexistent when using explicit deuterium atoms and very small and restricted to the fastest available time values for the dynamic data.

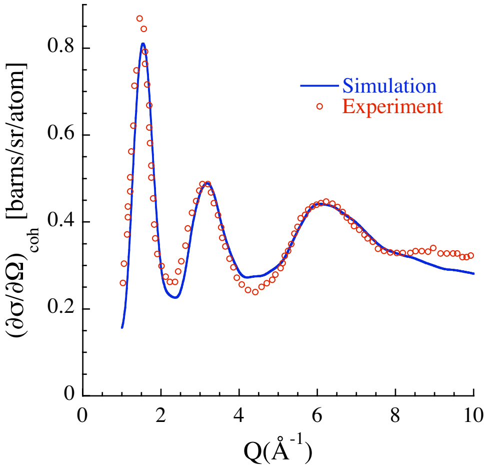

FIG. 5. (Color online) Static structure factor as calculated from MD simulations (line) and from neutron diffraction experiments with polarization analysis (symbols) (Ref. 60).

IV. VALIDATION OF THE SIMULATED SYSTEM

To justify any conclusions drawn from the simulation, we first have to validate the system. Therefore we used the full trajectories of the atoms to calculate functions that have been accessed with neutron scattering experiments. The validation is based on the direct comparison of different correlators accessing different aspects: First, the structure of the system will be verified by considering the static structure factor (diffraction measurements from literature[60]). Second, the self motions of the hydrogen atoms will be contrasted (FOCUS, backscattering). Lastly we check the results on collective dynamics (TOFTOF and NSE). All values calculated from the simulated system were averaged over the course of the simulation to create a statistically valid result.

A. Structure

In Fig. 5 the static structure factor of deuterated PEO as measured by neutron scattering[60] at a temperature of 363 K is compared with the simulation results at 350 K. The agreement is good and, indeed, similar to that displayed in Ref. 60 using a "polymerizing" simulation model.[40] Comparison of the protonated PEO system yields similar agreements. Thus, with these comparisons, we demonstrated that the short-range order in PEO is well reproduced by our simulated cell.

B. Dynamics

1. Self-motion

First we focus on the self-motion of the hydrogen atoms in the sample addressed experimentally on hPEO. Since experiments explore only the reciprocal space, the comparison between neutron scattering and simulation results is better realized through the intermediate scattering function $S_{\rm inc}^{\rm H}(Q,t)$. This can be computed from the simulations via Fourier transformation of the corresponding radial probability distribution function [Eq. (1)] into the Q-space,

$$S_{\rm inc}(Q,t) = \left\langle \int_{-\infty}^{\infty} d^3 r e^{i\vec{Q}\vec{r}} G_{\rm self}(\vec{r},t) \right\rangle_{\Omega}. \qquad (4)$$

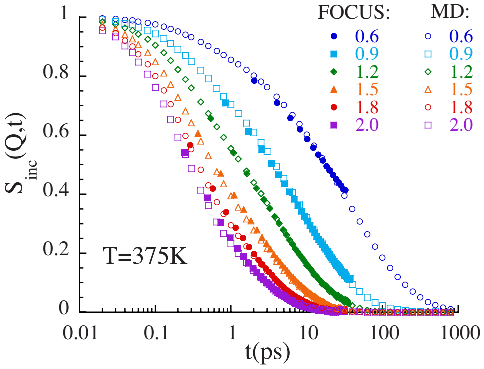

FIG. 6. (Color online) Direct comparison of the incoherent scattering functions calculated from MD simulations (empty symbols) with Fourier-transformed results from FOCUS measurements (full symbols) at $T = 375$ K and the Q-values indicated (units: Å^{-1}).

A direct comparison of FOCUS and simulation results is done in Fig. 6. As can be appreciated, the agreement between both sets of data is excellent. We have shown before for the FOCUS results (Fig. 1) that the KWW functional form with $\beta = 0.5$ describes very well the decay of the intermediate scattering function above ≈2 ps. This is also the case for the simulation data extended in a larger time window, as can be seen in Fig. 7. Underlining the consistency of the comparison, Fig. 8 shows the almost perfect agreement between the time scales deduced from such a parametrization of both ToF and simulation results. Now considering the backscattering results, we note that their Fourier transformation is not straightforward due to the rather limited dynamic window accessed by these instruments. Therefore, the backscattering data were directly fitted in the frequency domain with the Fourier transformed KWW function (β=0.5).[7,23] The corresponding results for the time scales have been included in Fig. 8. The agreement is excellent for all three temperatures. The dispersion law $\tau_W \propto Q^{-4}$ is thus very well established in the Q-range below ≈0.6 Å^{-1}. This dependence implies the Gaussian functional form of the intermediate scattering function and consequently of the self-part of the van Hove correlation function[69] and, as we will see below, it is compatible with Rouse-like dynamics.[70]

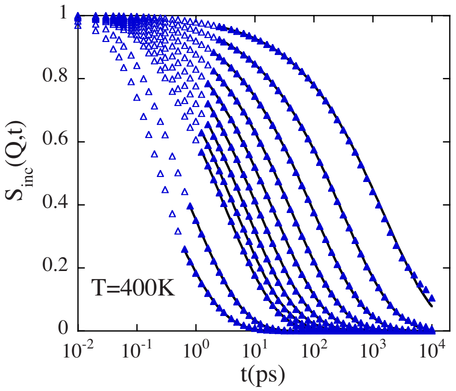

FIG. 7. (Color online) Incoherent intermediate scattering function, $S_{\text{inc}}(Q,t)$, as calculated from MD simulations for the hydrogen atoms of PEO. The curves correspond to the Q-values of 0.1, 0.2, 0.3, 0.4, 0.5, 0.6, 0.7, 0.8, 0.9, 1.0, 1.5, and 2.0 Å^{-1} (top to bottom). KWW fits with β=0.5 are displayed by the solid lines; in their fit, only the full symbols (times longer than ≈1 ps) have been considered.

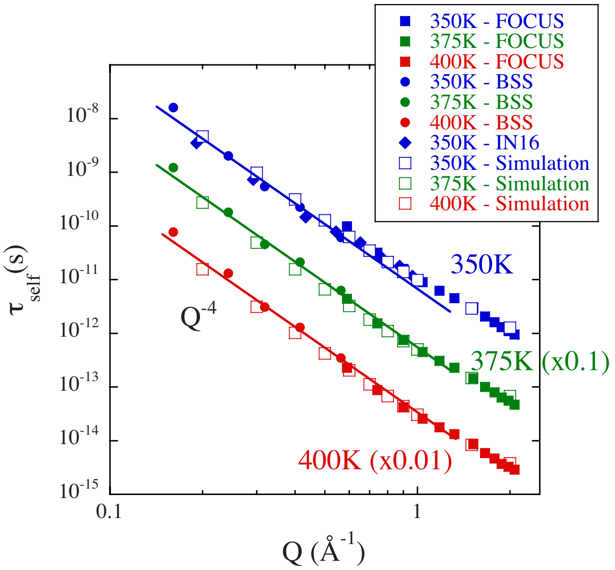

FIG. 8. (Color online) Momentum transfer dependence of the characteristic times τ_W obtained from the KWW fits of the incoherent intermediate scattering function. The empty symbols represent data from MD simulations, while the full symbols show experimental data [FOCUS (PSI), BSS (FZ-Jülich), and IN16 (Grenoble)]. For clarity points for T=375 K have been multiplied by 0.1 and points for T=400 K by a factor of 0.01. The solid lines show Q^{-4}-laws.

2. Collective dynamics

Figure 9 shows good agreement between the dynamic structure factor calculated from the MD simulations and measured on the deuterated sample by means of TOFTOF. The description of the simulated data in terms of stretched exponentials reveals coherent time scales that clearly show reminiscences of the structure factor. Figure 10 compares the ratio between the characteristic time scales deduced from the coherent scattering function and the incoherent scattering function corresponding to H-atoms as obtained from the MD simulations and the experiments. The same Q-dependence is observed for both sets of data. Extending to lower Q-values, the simulation results show a clear maximum centered at about 1.4 Å^{-1}. We also included the computed structure factor in the figure. The simple deGennes narrowing approach implies that the ratio of the time scales coincides with $S(Q)$.

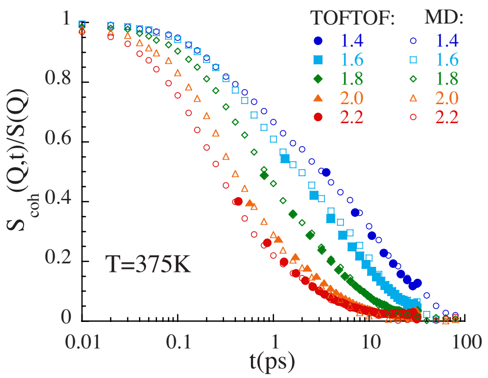

FIG. 9. (Color online) Direct comparison of the normalized dynamic structure factor $S_{\text{coh}}(Q,t)/S(Q)$ as calculated from MD simulations (empty symbols) and obtained through Fourier transformation of TOFTOF-measurements (full symbols). The shown scattering vectors are indicated in units of Å^{-1}.

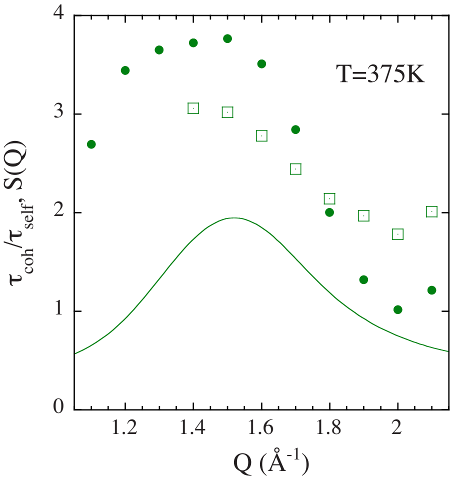

FIG. 10. (Color online) Momentum transfer dependence of the ratio between the coherent and incoherent characteristic times (full circles are from the MD simulations and empty squares are from TOFTOF) for 375 K. The line shows the static structure factor for comparison.

However, we note that (i) the values obtained for this ratio are clearly higher than $S(Q)$ in the whole range investigated and (ii) the maximum slowing down of the collective dynamics occurs at lower Q-values than the static structure peak. Observation (i) might be due to the faster self-motions of hydrogen atoms compared to the carbons and oxygens, which self-correlation function, though not experimentally accessible, also contributes to the self part of the van Hove correlation function in the fully deuterated sample. On the contrary, observation (ii), namely, the relative shift of the dynamic and static maxima, cannot be rationalized in terms of such kinds of arguments. Similar behavior has also been found in other polymer systems.[37,70,71] Obviously, the deGennes approach proposed for monoatomic simple liquids cannot be applied rigorously to more complex systems such as polymers.

As a general conclusion, from this thorough comparison, we can state that not only the self-motions of H-atoms but also the collective dynamics of PEO are well reproduced by the simulated cell. After this critical check of the reliability of the simulations, we can take advantage of them and calculate magnitudes that are experimentally not accessible.

V. DISCUSSION

A. Hydrogen motions: Real-space analysis

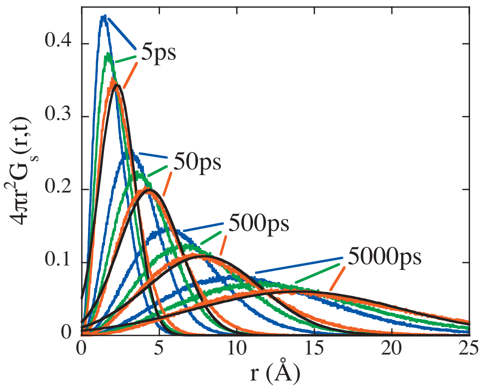

FIG. 11. (Color) Radial probability distribution functions obtained from the self-part of the van Hove correlation functions for PEO hydrogens at the three temperatures investigated (blue: 300 K, green: 375 K, and red: 400 K) at the different times indicated. Gaussian fits for the 400 K data are shown by black lines.

We will now focus on the dynamic behavior of atoms in the simulated system, in particular of the hydrogens, the motions of which can be experimentally addressed. Figure 11 shows the distribution of displacements for hydrogen atoms as a function of time and temperature. They are determined by the self-part of the van Hove correlation function $G_{\rm self}^{\rm H}(r,t)$ [Eq. (1)]; the function $4\pi r^2 G_{\rm self}^{H}(r,t)dr$ represents the probability of finding a hydrogen atom after time t between the distance r and $r+dr$ relative to its position at $t=0$. Looking at larger times the distribution shifts to higher displacements and is broadened. These are typical features of a diffusivelike behavior. The same happens for an increase in temperature. A Gaussian function,

$$G_{\rm self}^{\rm Gauss}(r,t) = \left(\frac{\alpha(t)}{\pi}\right)^{3/2} \exp[-\alpha(t)r^2], \tag{5}$$

can be used to describe the self-correlation function $G_{\rm self}^{H}(r,t)$ (black lines in Fig. 11). The slight deviations found from this Gaussian form can be parametrized in terms of the second order non-Gaussian parameter $\alpha_2(t)$, which can directly be calculated from the second ($\langle r^2(t)\rangle$) and fourth ($\langle r^4(t)\rangle$) moments of $G_{\rm self}^{\rm H}(r,t)$,

$$\alpha_2(t) = \frac{3}{5}\frac{\langle r^4(t)\rangle}{\langle r^2(t)\rangle^2} - 1. \tag{6}$$

For a perfect Gaussian curve, $\alpha_2(t)=0$. The time dependence of the parameter $\alpha_2(t)$ is shown in Fig. 12(a). For times $t < 1$ ps the three temperatures show very similar behavior, for times from 1 to 100 ps, they differ. For comparison, Fig. 12(b) shows the MSD $\langle r^2(t)\rangle$ of the H-atoms (second moment of the corresponding self-part of the van Hove correlation function). The values have been multiplied by a factor of 10 (375 K) and 100 (400 K) for clarity. After a rapid increase in $\langle r^2(t)\rangle$ in the microscopic region below $\approx$0.1 ps, we can see a transition to a regime where the MSD increases sublinearly with time as $\langle r^2(t)\rangle \propto t^{0.5}$ for $t \gtrsim 5$ ps. This regime is observed up to some 10^4 ps. In the microscopic region at short times the dynamics is dominated by the so-called "fast-process" still of controversial origin.[59] There the main peak of the non-Gaussian parameter is located (at $t\approx 0.1$ ps). The temperature-dependent second peak of $\alpha_2(t)$ around 1–10 ps (indeed a shoulder at 400 K) occurs in the crossover region from microscopic to subdiffusive behavior and we could attribute it to the local events leading to the decaging process (α-relaxation).[35] In previous works,[38,39,72,73] this peak has been interpreted as a signature of the existence of a distribution of discrete jumps underlying the atomic motions in the α-process. We note that in the high-temperature range explored for PEO, the decaging regime is very reduced and shows very small associated values of the $\alpha_2(t)$-parameter (less than 0.3). This implies that the deviations from Gaussian behavior should not be apparent. In fact, it has been reported that the deviations with respect to the $Q^{-2/\beta}$-dependence of the characteristic time (which corre-

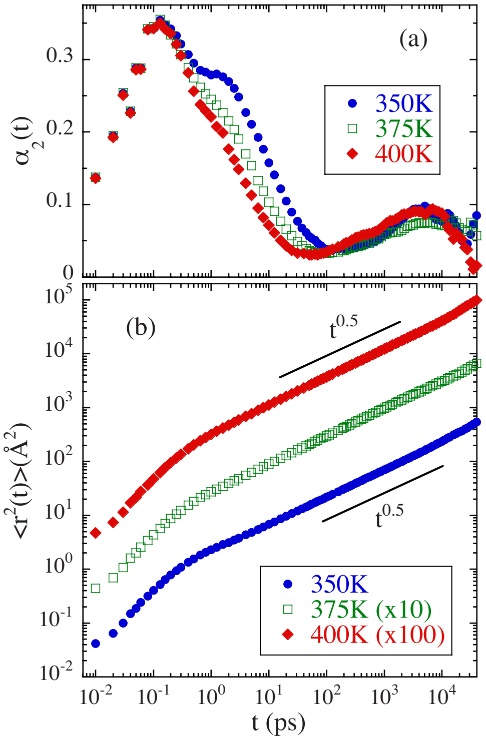

FIG. 12. (Color online) (a) Non-Gaussian parameter and (b) $\langle r^2(t)\rangle$ for the hydrogen atoms at the temperatures investigated. The values in (b) have been multiplied by a factor of 10 for $T=375$ K and 100 for $T=400$ K.

sponds to the Gaussian case in a subdiffusive motion[69]) are negligible for times at which the value of $\alpha_2(t)$ is lower than 0.2…0.3.[35,72,74] Consequently, the self-time scales of PEO (Figs. 2 and 8) should obey the $Q^{-2/\beta}$-law (i.e., $\tau_{\mathrm{self}} \propto Q^{-4}$) for times longer than about 10 ps. As can be observed in these figures, this is what is observed ($\tau_{\mathrm{self}} \gtrsim 10$ ps for Q-values smaller than ≈ 0.6 Å^{-1}). Thus, for the temperature range investigated, we can say that the decaging α-process in PEO has practically merged with the microscopic dynamics.

B. Rouse-mode analysis

1. Predictions of the Rouse model

In the following part we want to compare results of our simulations with predictions of the Rouse model. The Rouse model starts from a Gaussian chain representing a coarse grained polymer model where springs stand for the entropic forces between hypothetic beads.[75,76] We are interested in the motion of segments on a length scale $\ell < r < R_E$, where $R_E^2 = N\ell^2$ is the end to end distance of the chain and N is the number of beads in the chain. Each segment "i" is subject to an entropic force $\propto 3k_BT/\ell^2$ (k_B is the Boltzmann constant and T is the temperature) and to a stochastic force $\vec{f}_i(t)$, which fulfills $\langle \vec{f}_i(t)\rangle = 0$ and $\langle \vec{f}_{i\alpha}(t)\vec{f}_{j\beta}(t')\rangle = 2k_BT\zeta_0\delta_{ij}\delta_{\alpha\beta}\delta(t-t')$. ζ_0 denotes the friction coefficient and α,β denote he Cartesian components. Excluded volume effects are not taken into account. The Langevin equation for segment motion assumes the form

$$\zeta_0 \frac{\partial \vec{r}_i}{\partial t} = \frac{3k_BT}{\ell^2}[\vec{r}_{i+1}+\vec{r}_{i-1}-2\vec{r}_i]+\vec{f}_i(t). \tag{7}$$

The Langevin equation can then be solved by introducing normal coordinates $\vec{X}_p(t)=N^{-1}\Sigma_{i=1}^{N}\vec{r}_i(t)\cos[(i-1/2)p\pi/N]$ with the Rouse modes $p=0,\ldots,N-1$. The mode $p=0$ corresponds to the center of mass of the chain. Using this approach the behavior of the chain can be described by the Rouse correlators that are given by $(p,q>0)$:

$$\Phi_{pq} = \frac{\langle \vec{X}_p(t)\vec{X}_q(0)\rangle}{\langle \vec{X}_p^2(0)\rangle} \tag{8}$$

$$\langle \vec{X}_p(t)\vec{X}_q(0)\rangle = \frac{\ell^2}{8N\sin^2(p\pi/2N)}e^{-t/\tau_p}\delta_{pq} \tag{9}$$

where Φ_{pq} is the normalized Rouse correlator and the mode relaxation time τ_p is given by

$$\tau_p = \frac{\zeta_0\ell^2}{12k_BT\sin^2(p\pi/2N)}. \tag{10}$$

For small p we have

$$\tau_p = \frac{\tau_R}{p^2} = \frac{1}{W\pi^2}\left(\frac{N}{p}\right)^2; \quad W = \frac{3k_BT}{\ell^2\zeta_0}. \tag{11}$$

τ_R is the Rouse time (the longest time in the relaxation spectrum) and W is the elementary Rouse rate. For the center of mass coordinate one finds

$$\langle \vec{X}_0(t)\vec{X}_0(0)\rangle = \frac{6k_BT}{N\zeta_0}t. \tag{12}$$

This defines a Rouse diffusion coefficient as

$$D_R = \frac{1}{6t}\langle \vec{X}_0(t)\vec{X}_0(0)\rangle = \frac{k_BT}{N\zeta_0} = \frac{W\ell^4}{3R_E^2}. \tag{13}$$

2. Scattering from a Rouse chain

Scattering experiments relate to mean square segment correlation functions, which are obtained by back transformation of the normal coordinates,

$$\begin{aligned} B(n,m,t) &= \langle[\vec{X}_n(t)\vec{X}_m(0)]^2\rangle \\ &= 6D_Rt + |m-n|\ell^2 + \frac{4N\ell^2}{\pi^2}\sum_{p=1}^{N}\frac{1}{p^2} \\ &\quad \times\cos\left(\frac{p\pi m}{N}\right)\cos\left(\frac{p\pi n}{N}\right)\left[1-\exp\left(-\frac{tp^2}{\tau_R}\right)\right]. \end{aligned} \tag{14}$$

For the special case of the self-correlation function ($n=m$) $B(n,n,t)$ reveals the MSD of a polymer segment. For large enough p one obtains the famous square root of two time law,

$$\langle r^2(t)\rangle = 2\ell^2\left(\frac{3k_BTt}{\pi\zeta_o\ell^2}\right)^{1/2} + 6D_Rt. \tag{15}$$

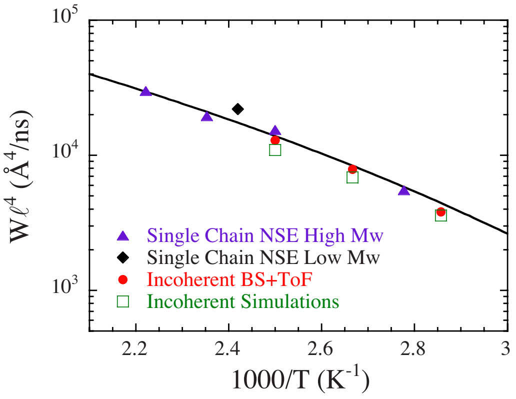

FIG. 13. (Color online) Temperature dependence of the Rouse rates obtained for PEO from different sources: NSE experiments on the single chain dynamics [triangles: high-molecular weight sample (Ref. 58), diamond: low-molecular weight sample (Ref. 58)], backscattering, and FOCUS experiments on fully protonated sample addressing H self-motions (circles) and our MD simulations (squares) (see the text). The solid line is a fit to a Vogel–Fulcher $\propto \exp[-B/(T-T_o)]$ law with the values $B = 1090$ K and $T_o = 155$ K given in Ref. 58.

The self-correlation function relates directly to the MSD of the diffusing segments. In Gaussian approximation for $t < \tau_R$ we have

$$
\begin{aligned}
S_{\mathrm{self}}(Q,t) &= \exp\left[-\frac{Q^2}{6}\langle r^2(t)\rangle\right] \\
&= \exp(-Q^2 D_R t)\exp\left[-\frac{2}{\sqrt{\pi}}\left(\frac{k_B T\ell^2}{12\zeta_0}Q^4 t\right)^{1/2}\right] \\
&= \exp(-Q^2 D_R t)\exp\left[-\left(\frac{W\ell^4 Q^4 t}{9\pi}\right)^{1/2}\right]. \qquad (16)
\end{aligned}
$$

For Q-values where the diffusion contribution is not important, Eq. (16) has just the form of a stretched exponential [Eq. (2)] with a shape parameter $\beta=0.5$ and a characteristic time

$$
\tau_{\mathrm{self}}^{\mathrm{Rouse}}(Q,t) = \frac{9\pi}{W\ell^4}Q^{-4}. \qquad (17)
$$

Interpreting the dynamic scattering data on PEO in terms of the Rouse model, we realize:

(1) The predicted Q-dependence of the characteristic relaxation time $\tau(Q) \propto Q^{-4}$ [Eq. (17)] is well fulfilled for Q values up to $Q \approx 0.6$ Å^{-1} (see Fig. 8).

(2) The measured incoherent scattering functions follow very precisely the prediction of Eq. (16) (see Figs. 6 and 7).

(3) The single chain dynamic structure factor from a $M_w = 2000$ g/mol PEO chain[58] follows also very well the Rouse prediction for this case.

(4) From the scattering data the characteristic Rouse variable $W\ell^4$ may be extracted [see Eq. (17)] and put into context with other experimental results. Figure 13 presents the result. Excellent internal consistency is achieved. We further note that in Ref. 58 some of these results were shown to quantitatively agree with friction coefficients obtained from short chain rheology.

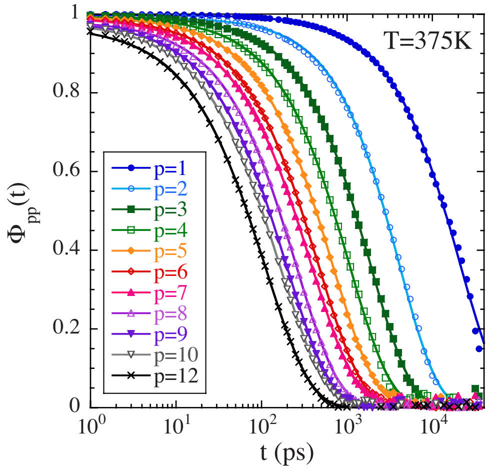

FIG. 14. (Color online) Normalized Rouse correlators $\Phi_{p,p}(t)$ for the modes $p=1,2,3,4,5,6,7,8,9,10,12$ using one monomer as bead. The solid lines show fits by stretched exponential functions.

In conclusion we may state that all scattering experiments available are in nearly perfect agreement with the prediction of the Rouse model.

3. Testing the Rouse prediction using the simulations

With simulation and experiments also agreeing well, we may now ask which additional information can be extracted from the simulation and which is not accessible experimentally. For that purpose we now perform a Rouse analysis of the simulations. In order to calculate the Rouse modes from the fully atomistic simulations, we have to perform some coarse graining in connecting several atoms to create one bead. Here, we take the center of mass of one monomer as one bead creating 43 modes ($p=0\ldots42$, the simulated PEO consists of 43 monomers). The Rouse model predicts orthogonality for the correlators $\langle \vec{X}_p(0)\vec{X}_q(0)\rangle$. With our choice of the bead, the condition $|\langle \vec{X}_p(0)\vec{X}_q(0)\rangle| \ll 1$ is nearly always fulfilled. Only for very short wavelengths or high mode numbers some deviations are found.

Next we can test the exponentiality of the Rouse modes. Figure 14 shows the normalized correlators $\Phi_{pp}(t)$ for some of the first modes at $T=400$ K in a time range of up to 40 ns. The data are fitted with a stretched exponential [Eq. (2)] describing their decay.

Figures 15(a)–15(c) show the dependence of the average relaxation time $\langle\tau\rangle = \tau_W \Gamma(1/\beta)/\beta$, the stretching parameter β, and the mode amplitudes $\langle X_p^2(0)\rangle$ in dependence of N/p and T. For smaller p, the relaxation times τ_p show the expected $\propto 1/p^2$ behavior and the solid lines display this prediction of the Rouse model. For p-values above ≈ 20 the obtained mode relaxation times tend to be faster than Rouse indicating that at wavelengths corresponding to about two to three beads or less the validity of the model is limited. From the first mode $p = 1$ we may read off the Rouse time τ_R. For $T=400$ K, we get $\tau_R = 12.4$ ns comparing favorably with the experimental value of $\tau_R = 14.7$ ns at this temperature. Figure 15(b) shows that for long wavelengths or small p the

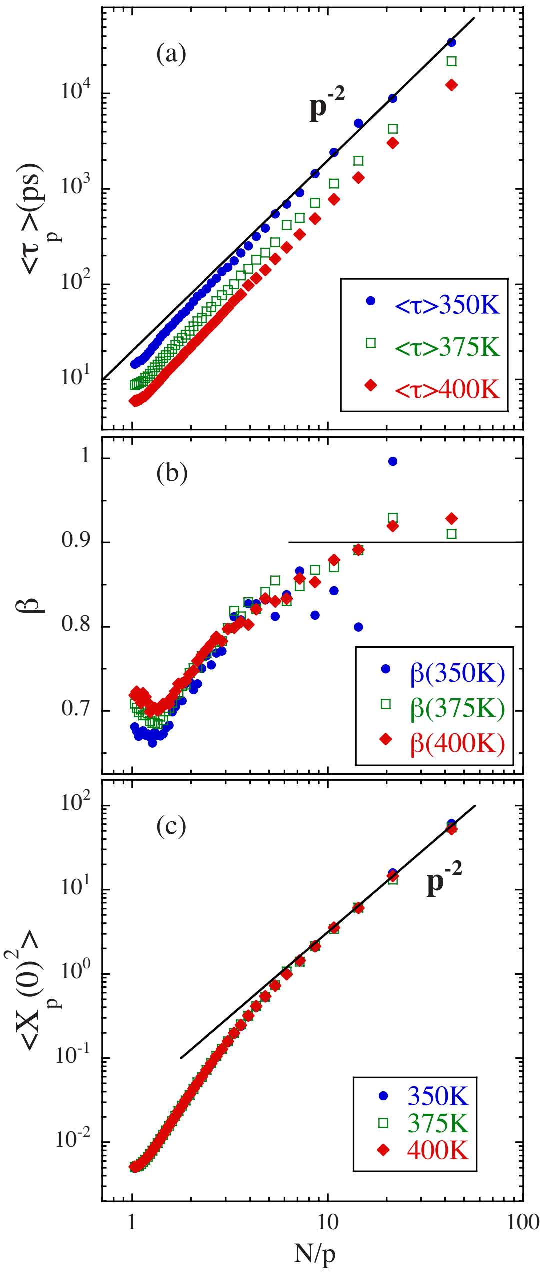

FIG. 15. (Color online) Mode-wavelength dependence of the fitting parameters obtained for the KWW descriptions of the Rouse-mode correlators at the different temperatures investigated: (a) average time $\langle \tau_p \rangle$ and (b) shape parameter β. The mode amplitudes are depicted in panel (c). The line in (b) shows the asymptotic value of the shape parameter, while in (a) and (c) it indicates the mode number dependence predicted by the Rouse model in the low-p range.

stretching parameters have values of $\beta \approx 0.9$ confirming an almost exponential behavior. They show no dependence on the temperature. For high p-values a more nonexponential behavior is observed, which indicates some influence from local potentials at shorter wavelength, in agreement with the deviations from $1/p^2$ shown by the relaxation times. The mode amplitudes, presented in Fig. 15(c), display an analogous behavior: For small p up to about $p = 8$ they follow the $1/p^2$ Rouse prediction while for larger p the amplitudes are massively suppressed indicating significantly stronger restoring forces than those originating from the entropic potential. We note that the deviations from the Rouse predictions are most pronounced for the mode amplitudes where they occur also at the lowest mode numbers, while the characteristic relaxation times follow the predicted $1/p^2$ behavior to significantly larger p.

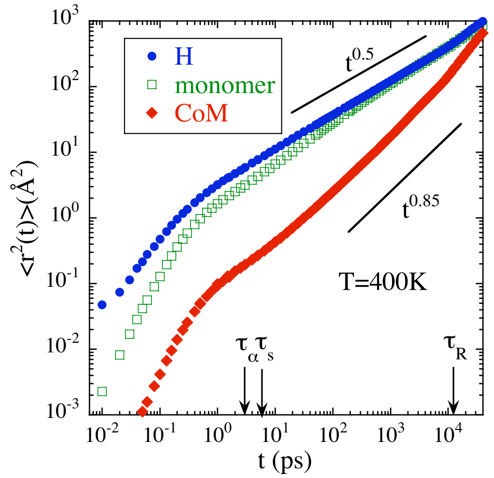

FIG. 16. (Color online) MSD of the H-atoms (circles), of the blob (monomer) (squares), and of the center of mass of the chain (diamonds) at 400 K. The vertical arrows indicate the Rouse time ($\tau_R = 12.4$ ns), the segmental time ($\tau_s = \tau_R/(N-1)^2 = 7$ ps), and the structural relaxation time $\tau_\alpha = 3$ ps.

Finally, Fig. 16 displays the simulation results for the time dependent center of mass MSD for $T = 400$ K. Also included are the MSD of the hydrogen atoms (seen by the neutrons) and those of the blobs (monomer center of mass). An arrow indicates the Rouse time $\tau_R = 12.4$ ns. We note that, other than predicted, the center of mass MSD grows sublinearly with time indicating sublinear diffusion behavior, a phenomenon already observed in earlier experimental and simulation work on polybutadiene[77] and lately on polyethylene melts.[78] We also see that at early times the atomic displacements show different time dependences, with the hydrogen displacements larger than those of the monomers. It is only when the total MSD becomes larger than the lateral size of the chain that all atomic displacements follow the same time law. On the other hand, we realize that the segmental time τ_s (corresponding to the shortest mode in the chain) is slightly slower than the structural relaxation time τ_α. This time τ_α, defined as that where the normalized dynamic structure factor $S_{\mathrm{coh}}(Q,t)/S(Q)$ reaches the value $1/e$, determines the decay of the intermolecular correlations and characterizes the α-relaxation. As previously commented, in our temperature range the decaging mechanism leading to the relaxation of the structure in PEO takes place at time scales very close to the microscopic regime ($\tau_\alpha = 3$ ps). We are thus witnessing an almost direct crossover from the fast dynamics to the Rouse regime at these high temperatures.

4. Rationalization of the results

From a conceptual point of view this model is limited toward smaller scales, where the simplifying assumptions of the Rouse model cease to be valid and the local chain structure comes into play. Locally the chain is stiff and this rigidity leads to deviations from the Rouse model. Furthermore, as a consequence of the rotational potentials, relaxation mechanisms across the rotational barriers come into play

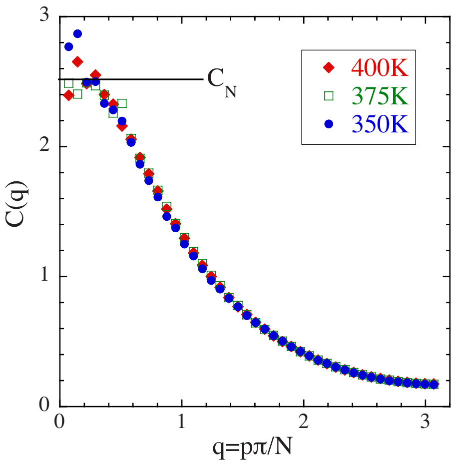

FIG. 17. (Color online) Mode-wavelength dependence of the characteristic ratio calculated from the coarse grained chain at the three temperatures investigated.

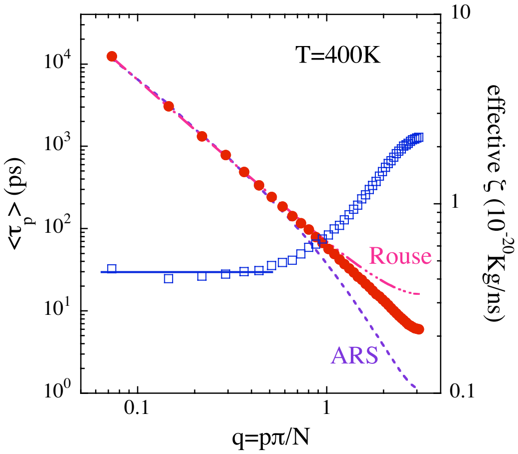

FIG. 18. (Color online) Mode-wavelength dependence of the average characteristic times obtained from KWW fits of the modes (circles) compared with the Rouse (dashed-dotted line) and the ARS (dotted line) predictions. The squares show the effective monomeric friction coefficient ζ_{eff} deduced (see the text). The horizontal solid line indicates the experimental ζ-value (Ref. 58).

leading to additional friction. Similarly specific local chain interactions may add to this additional friction.

As was shown by Flory,[79] in a real chain segment-segment correlations extend beyond nearest neighbor distances. The standard model to treat the local statistics would be the rotational isomeric state (RIS) formalism. For a mode description, as it is required for an evaluation of the chain motion, it is more appropriate to consider the so-called all rotational state (ARS) model,[80] which describes the chain statistics in terms of orthogonal Rouse modes. In the ARS approach the characteristic ratio C_∞ of the RIS model becomes mode dependent $[C(q=\pi p/N)]$ and as a function of the mode number assumes a bell shaped form with $C(0)=C_\infty$. The mode dependence leads to a stiffening of the chain for higher q, where $C(q)$ drops and consequently the spring constant increases. The mode-relaxation times become

$$\tau(q)=\frac{\zeta_0 b_0^2 C(q)}{12k_BT\sin^2(q/2)}, \tag{18}$$

where in our case b_0^2 is the average squared coarse grained "bond length." In the low q (low p) limit $C(q)\to C_\infty$ and $\tau(q)$ assume the standard Rouse form [Eq. (10)]. As soon as q increases $C(q)$ reduces and the amplitudes of the modes should also drop. Now we apply this approach to our simulation results. We may independently calculate

- the mode amplitudes telling us about the restoring forces and
- the mode relaxation times, which also include the friction.

First from the amplitudes we obtain $C(q)$. In order to get absolute numbers, we need to remember that we coarse grained the simulations taking one monomer as a bead size. For the corresponding bead size b_0^2 the simulations give 10.14 Å^2. Thus

$$\langle X_p^2(0)\rangle=\frac{\ell^2}{8N\sin^2(q/2)}=\frac{b_0^2C(q)}{8N\sin^2(q/2)}. \tag{19}$$

Figure 17 shows the result. Indeed a bell shaped curve is obtained. For the low q limit we get $C(0)=\ell^2/b_0^2=C_N\approx 2.5$, a characteristic ratio reflecting the coarse grained nature of the chain.

If the increasing local stiffness is the only reason for the deviations of τ_p from the Rouse form [Eq. (10)], then an application of the results for $C(q)$ in Eq. (18) should rectify the deviations and lead to the proper predictions for τ_p. Figure 18 displays a comparison of the measured τ_p with the Rouse predictions of Eq. (10) and the ARS prediction of Eq. (18). It is obvious that the ARS model is not accounting for the observed p-dependence. While the Rouse prediction lies above the simulated τ_p, the ARS results are significantly below. Thus it seems that a further mechanism compensating the local stiffness needs to be taken into account. Inspecting Eq. (18) suggests to postulate a p-dependent friction, which counteracts the stronger restoring forces at high p. The resulting p-dependence of the friction coefficient is also included in Fig. 18 and shows a strong increase with p above $p\approx 8$.

Qualitatively similar effects were already observed experimentally in polyisobutylene (PIB) melts,[81] and also in PIB solutions,[82] and interpreted in terms of an internal viscosity model by Allegra and Ganazzoli.[83] However in detail the phenomenology of the effect is different for PEO. While for PIB a mode damping was found commencing already for low p modes, here the effect remains restricted to high p. Furthermore, in the case of PIB the additional friction leads to an overall weaker dependence than $1/p^2$ of the Rouse modes, while here the modes still decay stronger than $1/p^2$. This qualitatively different behavior may result from the very different rotational potentials, which are very weak in PEO but very strong in PIB, causing very different internal viscosities.

Finally, addressing the sublinear center of mass diffusion, we relate to the mode coupling approach of Guenza.[84] While in the Rouse theory intermolecular interactions are ignored, more realistically in a polymer melt a chain spanning a volume $V\approx R_g^3$ (R_g the chain radius of gyration) may interact with the $n \approx \sqrt{N}$ other chains that on average fill the volume of a given chain. In Guenza's approach[84] the pair interaction potential is repulsive and Gaussian in shape with a small attractive tail and a range on the order of R_g. The strength of the pair potential is $\approx 1/\sqrt{N}$, which taking into account the number of interacting polymer pairs leads to a N-independent total strength of the potential, suggesting that intermolecular effects should be relevant at any molecular weight. Solution of the corresponding generalized Langevin equation leads to subdiffusive center of mass motion. Explicit calculations for paraffins between 10 and 96 carbons gave time exponents $0.85 \leq \beta \leq 0.97$. These predictions were validated by simulations of paraffin melts[85] and are within the range of our results.

VI. CONCLUSIONS

In this work we presented a detailed comparison of MD simulations and quasielastic neutron scattering results of a PEO melt. Furthermore, the simulated short-range order as presented by the structure factor was validated by a structure factor measurement. We found very good agreement between simulations and both the structural as well as the dynamic experimental data. After this validation we performed a further analysis of the simulation data.

The following results stand out:

- In real space the hydrogen self-correlation function follows very well a Gaussian distribution. The second-order non-Gaussian parameter was found to be very close to zero for times beyond the microscopic dynamics. This is also reflected in the Q-dependence of the characteristic relaxation time, which for Q-values smaller than 0.6 Å^{-1} is proportional to Q^{-4}.
- An analysis of the neutron scattering data in terms of the Rouse model revealed nearly perfect agreement between model and experimental results up to a Q-range of about 0.6 Å^{-1}. This concerns the Q-dependence of the characteristic times, the single chain dynamic structure factor, the incoherent scattering functions, as well as the absolute value of the Rouse variable in the context of published data.
- Using the simulations, the Rouse predictions were tested further. In particular it was possible to extract independently the mode amplitudes, the characteristic relaxation times, and the shape of the Rouse correlators. It was shown that the deviations occurring at larger mode numbers cannot be explained by a local stiffness alone but require a significant increase in the mode friction for higher mode numbers.
- Finally, the simulation shows a sublinear center of mass diffusion, which could be rationalized in terms of the interchain potential proposed by Guenza (Ref. 85).

In summary, the MD simulation based on the COMPASS force field including a proper treatment of the long-range Coulomb interaction yields a quantitative agreement with quasielastic neutron scattering results establishing a quantitative valid computer model for this important polymer.

ACKNOWLEDGMENTS

We thank A. C. Genix for experimental help in FOCUS. This work is partially based on experiments performed at the Swiss spallation neutron source SINQ, Paul Scherrer Institute, Villigen, Switzerland. This research project was supported by the European Commission NoE SoftComp under Contract No. NMP3-CT-2004-502235 and the "Donostia International Physics Center." A.A., F.A., and J.C. acknowledge support from Project Nos. MAT2007-63681 and IT-436-07 (GV) and the Spanish Ministerio de Educacion y Ciencia (Grant No. CSD2006-53).

[1] F. M. Gray, *Polymer Electrolytes* (Royal Society of Chemistry, Cambridge, UK, 1997).
[2] P. G. Bruce and C. A. Vincent, J. Chem. Soc., Faraday Trans. **89**, 3187 (1993).
[3] R. Ramachandran, Plastics Eng. **52**, 31 (1996).
[4] S. A. Altaf, S. W. Hoag, and J. W. Ayres, Drug Dev. Ind. Pharm. **24**, 737 (1998).
[5] R. Gutzler, M. Smulders, and R. F. Lange, Macromol. Symp. **225**, 81 (2005).
[6] M. Dionísio, A. C. Fernandes, J. F. Mano, N. T. Correia, and R. C. Sousa, Macromolecules **33**, 1002 (2000).
[7] A.-C. Genix, A. Arbe, F. Alvarez, J. Colmenero, L. Willner, and D. Richter, Phys. Rev. E **72**, 031808 (2005).
[8] R. H. Colby, Polymer **30**, 1275 (1989).
[9] C. Lartigue, A. Guillermo, and J. P. Cohen-Addad, J. Polym. Sci., Part B: Polym. Phys. **35**, 1095 (1997).
[10] T. R. Lutz, Y. He, M. D. Ediger, H. Cao, G. Lin, and A. A. Jones, Macromolecules **36**, 1724 (2003).
[11] H. Cao, G. Lin, and A. A. Jones, J. Polym. Sci., Part B: Polym. Phys. **43**, 2433 (2005).
[12] X. Jin, S. Zhang, and J. Runt, Macromolecules **37**, 8110 (2004).
[13] K. L. Ngai and C. M. Roland, Macromolecules **37**, 2817 (2004).
[14] V. G. Sakai, C. Chen, J. K. Maranas, and Z. Chowdhuri, Macromolecules **37**, 9975 (2004).
[15] B. Farago, C. Chen, J. K. Maranas, S. Kamath, R. H. Colby, A. J. Pasquale, and T. E. Long, Phys. Rev. E **72**, 031809 (2005).
[16] V. García Sakai, J. K. Maranas, Z. Chowdhuri, I. Peral, and J. R. D. Copley, J. Polym. Sci., Part B: Polym. Phys. **43**, 2914 (2005).
[17] J. C. Haley and T. P. Lodge, J. Chem. Phys. **122**, 234914 (2005).
[18] T. P. Lodge, E. R. Wood, and J. C. Haley, J. Polym. Sci., Part B: Polym. Phys. **44**, 756 (2006).
[19] K. Niedzwiedz, A. Wischnewski, M. Monkenbusch, D. Richter, A.-C. Genix, A. Arbe, J. Colmenero, M. Strauch, and E. Straube, Phys. Rev. Lett. **98**, 168301 (2007).
[20] I. Zeroni, S. Ozair, and T. P. Lodge, Macromolecules **41**, 5033 (2008).
[21] A. N. Gaikwad, E. R. Wood, T. Ngai, and P. Lodge, Macromolecules **41**, 2502 (2008).
[22] I. Zeroni and T. P. Lodge, Macromolecules **41**, 1050 (2008).
[23] M. Tyagi, A. Arbe, J. Colmenero, B. Frick, and J. R. Stewart, Macromolecules **39**, 3007 (2006).
[24] M. Tyagi, A. Arbe, A. Alegrría, J. Colmenero, and B. Frick, Macromolecules **40**, 4568 (2007).
[25] M. A. Mazo, L. I. Manevitch, E. B. Gusarova, M. Y. Shamaev, A. A. Berlin, N. K. Balabaev, and G. C. Rutledge, J. Chem. Phys. **112**, 3579 (2008).
[26] K. Chrissopoulou, A. Afratis, S. H. Anastasiadis, M. M. Elmahdy, G. Floudas, and B. Frick, Eur. Phys. J. Spec. Top. **141**, 267 (2007).
[27] H. Furuya, M. Mondello, H.-J. Yang, R.-J. Roe, R. W. Erwin, C. C. Han, and S. D. Smith, Macromolecules **27**, 5674 (1994).
[28] D. J. Ward and G. R. Mitchell, Phys. Scr., T **t57**, 153 (1995).
[29] J. Eilhard, A. Zirkel, W. Tschöp, O. Hahn, K. Kremer, O. Schärpf, D. Richter, and U. Buchenau, J. Chem. Phys. **110**, 1819 (1999).
[30] F. Alvarez, J. Colmenero, R. Zorn, L. Willner, and D. Richter, Macromolecules **36**, 238 (2003).
[31] I. Iradi, F. Alvarez, J. Colmenero, and A. Arbe, Physica B **350**, e881 (2004).
[32] A. Narros, A. Arbe, F. Alvarez, J. Colmenero, R. Zorn, W. Schweika, and D. Richter, Macromolecules **38**, 9847 (2005).
[33] A.-C. Genix, A. Arbe, F. Alvarez, J. Colmenero, W. Schweika, and D.

Richter, Macromolecules **39**, 3947 (2006).
[34] N. E. Moe and M. D. Ediger, Phys. Rev. E **59**, 623 (1999).
[35] J. Colmenero, F. Alvarez, and A. Arbe, Phys. Rev. E **65**, 041804 (2002).
[36] J. Colmenero, F. Alvarez, A. Arbe, A. Narros, M. Monkenbusch, and D. Richter, Europhys. Lett. **71**, 262 (2005).
[37] A.-C. Genix, A. Arbe, F. Alvarez, J. Colmenero, B. Farago, A. Wischnewski, and D. Richter, Macromolecules **39**, 6260 (2006).
[38] A. Arbe, J. Colmenero, F. Alvarez, M. Monkenbusch, D. Richter, B. Farago, and B. Frick, Phys. Rev. Lett. **89**, 245701 (2002).
[39] A. Arbe, J. Colmenero, F. Alvarez, M. Monkenbusch, D. Richter, B. Farago, and B. Frick, Phys. Rev. E **67**, 051802 (2003).
[40] B. Lin, P. T. Boinske, and J. W. Halley, J. Chem. Phys. **105**, 1668 (1996).
[41] A. Maitra and A. Heuer, Macromol. Chem. Phys. **208**, 2215 (2007).
[42] V. Kuppa and E. Manias, J. Chem. Phys. **118**, 3421 (2003).
[43] C. Chen, P. Depa, V. G. Sakai, J. K. Maranas, J. W. Lynn, I. Peral, and J. R. D. Copley, J. Chem. Phys. **124**, 234901 (2006).
[44] G. D. Smith, O. Borodin, and D. Bedrov, J. Comput. Chem. **107**, 10446 (2003).
[45] O. Borodin and G. D. Smith, J. Phys. Chem. B **107**, 6801 (2003).
[46] G. D. Smith, R. L. Jaffe, and D. Y. Yoon, J. Phys. Chem. **97**, 12752 (1993).
[47] O. Borodin, G. D. Smith, and R. Douglas, J. Phys. Chem. B **107**, 6824 (2003).
[48] S. Neyertz, D. Brown, and J. O. Thomas, J. Chem. Phys. **101**, 10064 (1994).
[49] A. van Zon, B. Mos, P. Verkerk, and S. W. de Leeuw, Electrochim. Acta **46**, 1717 (2001).
[50] D. Rigby, H. Sun, and B. E. Eichinger, Macromolecules **44**, 311 (1998).
[51] O. Borodin and G. D. Smith, Macromolecules **31**, 8396 (1998).
[52] O. Borodin and G. D. Smith, Macromolecules **33**, 2273 (2000).
[53] S. Neyertz and D. Brown, J. Chem. Phys. **102**, 9725 (1995).
[54] G. D. Smith, D. Bedrov, and O. Borodin, Phys. Rev. Lett. **85**, 5583 (2000).
[55] J. W. Halley, Y. Duan, B. Nielsen, P. C. Redfern, and L. A. Curtiss, J. Chem. Phys. **115**, 3957 (2001).
[56] B. K. Annis, G. D. Smith, and C. J. Benmore, J. Chem. Phys. **115**, 10998 (2001).
[57] M. Fuson and M. D. Ediger, Macromolecules **30**, 5704 (1997).
[58] K. Niedzwiedz, A. Wischnewski, W. Pyckhout-Hintzen, J. Allgaier, D. Richter, and A. Faraone, Macromolecules **41**, 4866 (2008).
[59] R. Zorn, A. Arbe, J. Colmenero, B. Frick, D. Richter, and U. Buchenau, Phys. Rev. E **52**, 781 (1995).
[60] J. A. Johnson, M.-L. Saboungi, D. L. Price, S. Ansell, T. P. Russell, J. W. Halley, and B. Nielsen, J. Chem. Phys. **109**, 7005 (1998).
[61] P. G. de Gennes, Physica (Utrecht) **25**, 825 (1959).
[62] F. Mezei, *Neutron Spin Echo, Lecture Notes in Physics* (Springer Verlag, Heidelberg, 1980), Vol. 28.
[63] H. Sun, Macromolecules **28**, 701 (1995).
[64] H. Sun, J. Phys. Chem. B **102**, 7338 (1998).
[65] M. Allen and D. Tildesley, *Computer Simulation of Liquids* (Oxford University Press, Oxford, 1987).
[66] D. N. Theodorou and U. W. Suter, Macromolecules **19**, 139 (1986).
[67] D. N. Theodorou and U. W. Suter, Macromolecules **19**, 379 (1986).
[68] The dynamic structure factor at the first peak decays completely in the time of the simulations.
[69] J. Colmenero, A. Alegría, A. Arbe, and B. Frick, Phys. Rev. Lett. **69**, 478 (1992).
[70] D. Richter, M. Monkenbusch, A. Arbe, and J. Colmenero, *Neutron Spin Echo Investigations on Polymer Dynamics, Advances in Polymer Science* (Springer Verlag, Berlin, Heidelberg, New York, 2005), Vol. 174.
[71] B. Farago, A. Arbe, J. Colmenero, R. Faust, U. Buchenau, and D. Richter, Phys. Rev. E **65**, 051803 (2002).
[72] J. Colmenero, A. Arbe, F. Alvarez, M. Monkenbusch, D. Richter, B. Farago, and B. Frick, J. Phys.: Condens. Matter **15**, S1127 (2003).
[73] A. Narros, F. Alvarez, A. Arbe, J. Colmenero, D. Richter, U. Buchenau, and B. Farago, J. Chem. Phys. **121**, 3282 (2004).
[74] J. Colmenero, A. Arbe, F. Alvarez, A. Narros, D. Richter, M. Monkenbusch, and B. Farago, Pramana, J. Phys. **63**, 25 (2004).
[75] P. E. Rouse, J. Chem. Phys. **21**, 1272 (1953).
[76] M. Doi and S. F. Edwards, *The Theory of Polymer Dynamics* (Oxford University, Oxford, UK, 1986).
[77] G. D. Smith, W. Paul, M. Monkenbusch, L. Willner, D. Richter, X. H. Qiu, and M. D. Ediger, Macromolecules **32**, 8857 (1999).
[78] M. Zamponi, A. Wischnewski, M. Monkenbusch, L. Willner, D. Richter, P. Falus, B. Farago, and M. G. Guenza, J. Phys. Chem. B **112**, 16220 (2008).
[79] P. J. Flory, *Statistical Mechanics of Chain Molecules* (Interscience, New York, 1969).
[80] S. Brueckner, Macromolecules **14**, 449 (1981).
[81] D. Richter, M. Monkenbusch, J. Allgaier, A. Arbe, J. Colmenero, B. Farago, Y. Cheol Bae, and R. Faust, J. Chem. Phys. **111**, 6107 (1999).
[82] A. Arbe, M. Monkenbusch, J. Stellbrink, D. Richter, B. Farago, K. Almdal, and R. Faust, Macromolecules **34**, 1281 (2001).
[83] G. Allegra and F. Ganazzoli, Macromolecules **14**, 1110 (1981).
[84] M. Guenza, J. Chem. Phys. **110**, 7574 (1999).
[85] M. Guenza, Phys. Rev. Lett. **88**, 025901 (2001).